濟州大學校 尖端技術硏究所 論文集, 第17卷, 2號, pp.25-32, 2006. 12
Cheju Nat'l Univ. Res. Inst. Adv. Tech. Jour., Vol.17, No.2, pp.25-32, 2006. 12

# 전기 임피던스 단층촬영에서 비정적 타원형 경계면 추정을 위한 운동모델

우머 지샨 이자즈* · 김 경 연**

# Kinematic Models for Non-stationary Elliptic Region Boundaries in Electrical Impedance Tomography

Umer Zeeshan Ijaz* · Kyung-Youn Kim**

## ABSTRACT

In this study, we propose kinematic models for dynamic electrical impedance tomography(EIT) shape estimation of regions of known resistivities based on extended Kalman filter(EKF). The EIT inverse problem is formulated as a state estimation problem in which the system is modeled with the state equation and the observation equation. We are especially interested in the estimation of shape of air bubbles and conductive liquid in the industrial process pipelines. The proposed kinematic models are tested with computer simulations. From the simulations, we achieve a promising performance of this approach.

**Key Words** : Electrical impedance tomography, Kalman filtering

## 1. Introduction

In EIT, weak alternating currents are injected into the object via an array of disjoint contact electrodes attached on the exterior surface of the object. The objective is to estimate the resistivity distribution inside the object based on the voltage measurements that are needed to maintain the currents.

Some of the applications of EIT include geophysics, nondestructive evalution, industrial process monitoring, medical imaging etc. In geophysics, EIT can be used for delineating lithologic units(e.g., sands versus clays), monitoring emplacement and performance of subsurface barriers: permeable, flow-through type as well as impermeable, mapping the position of fluids such as water, mapping moisture content variation in space and time, detecting leaks in surface and subsurface storage tanks etc.

* 제주대학교 대학원
Graduate School, Cheju Nat'l Univ.
** 제주대학교 전기전자공학부
Faculty of Electrical & Electronic Eng., Cheju Nat'l Univ.

In many applications the object is known to consist of a few separate subregions with constant resistivities. In these situations the shape estimation techniques are the desired framework for the reconstruction. In shape estimation techniques the reconstruction is defined in terms of the shape of the subregion boundaries. With a shape parametrization we have less unknown parameters compared with the traditional pixelwise parameterization and hence it leads to less ill-posed estimation problem and improved accuracy in reconstructions. Latest research in shape estimation techniques are given in [1],[2],[3],[4], [5] and [6].

There are two types of boundary estimation problems. For the first case, object domain is divided into two disjoint regions which are separated by an open boundary [7]. In the other case the anomalies are enclosed by the background substance. Here the problem is the recovery of closed boundaries of subregions that are embedded in the object domain [8]. In [3] and [8] researchers have expressed the shape of interface in terms of Fourier series whose coefficients are the unknowns to be estimated. In this paper we propose kinematic models for state estimation. The object domain is assumed to consist of two disjoint regions, for example an air bubble in water. An important topic is the use of more appropriate evolution models in shape estimation. Such an evolution model can be constructed using first- and second-order Markov models. In this paper we give extensive simulations for different kinematic models incorporated into state estimation.

## 2. Expression of Phase Boundaries

We assume that the outer boundary of the body, that is, $\partial\Omega$ is known. If the phase boundaries of the object are sufficiently smooth, they can be approximated in the form

$$C_l(s) = \begin{pmatrix} x_l(s) \\ y_l(s) \end{pmatrix} = \sum_{n=1}^{N_\theta} \begin{pmatrix} \gamma_n^x \theta_n^x(s) \\ \gamma_n^y \theta_n^y(s) \end{pmatrix} \tag{1}$$

where $C_l(s)\ (l=1,2,\ldots,S)$ is the boundary of the $l$th object, $S$ is the number of the objects in the body, $\theta_n(s)$ are periodic and differentiable basis functions, and $N_\theta$ is the number of basis functions. In this paper, we express the phase boundaries as Fourier series in the two-dimensional coordinates with respect to the parameter $s$, that is, we use the basis function of the form

$$\begin{aligned} &\theta_1^\alpha(s) = 1 \\ &\theta_n^x(s) = sin(2\pi\frac{n}{2}s),\ n=2,4,6,\ldots,N_\theta-1 \\ &\theta_n^y(s) = cos(2\pi\frac{(n-1)}{2}s),\ n=1,3,5,\ldots,N_\theta \end{aligned} \tag{2}$$

where $s \in [0,1]$ and $\alpha$ denotes either $x$ or $y$. Furthermore, using the expansion Eq. (1), the boundaries are identified with vector $\gamma$ of the shape coefficients, that is,

$$\begin{aligned} \gamma = (&\gamma_1^{x_1},\ldots,\gamma_{N_\theta}^{x_1},\gamma_1^{y_1},\ldots,\gamma_{N_\theta}^{y_1},\ldots,\ldots, \\ &\gamma_1^{x_s},\ldots,\gamma_{N_\theta}^{x_s},\gamma_1^{y_s},\ldots,\gamma_{N_\theta}^{y_s})^T \end{aligned} \tag{3}$$

where $\gamma \in \mathbb{R}^{2sN_\theta}$. For more details on the expression of phase boundaries, Forward Model and implementation issues in FEM, see [9].

## 3. Formulation of Dynamic Model

In general, the evolution of the boundary vector $\gamma$ is related by the following nonlinear mapping;

$$\gamma_{k+1} = g_k(\gamma_k) + w_k \tag{4}$$

where $\gamma_k$ is the state vector (the boundary representation) at time $kT$. $g_k$ is a function ($g_k : \mathbb{R}^{2SN_\theta} \rightarrow \mathbb{R}^{2SN_\theta}$) defining the state transition from time $kT$ to $(k+1)T$, where $T$ is the sampling period (measurement interval between successive application of current patterns), and $w_k$ is assumed to be white Gaussian noise. Here, the state equation is assumed to be of linear form

$$\gamma_{k+1} = F_k\gamma_k + w_k \tag{5}$$

where $F_k \in \mathbb{R}^{2SN_\theta \times 2SN_\theta}$ is the state transition matrix at time $kT$. Usually in EIT there is no a priori information on the time evolution of the boundary vector so that we take $F_k \equiv I$ (the identity matrix). The rate of time evolution is governed by the covariance matrix $Q_k$. Considering the observation model, let $\bar{u} \in \mathbb{R}^L$, be defined as

$$\bar{u}_k \equiv (\bar{u}_k^1, \bar{u}_k^2, \ldots, \bar{u}_k^L)^T \tag{6}$$

be the actual surface measurement voltages induced by the $k$th current pattern. Then the relationship between the boundary vector and measured voltages can be described by the following nonlinear mapping with a measurement error

$$\bar{u}_k = h_k(\gamma_k) + v_k \tag{7}$$

where $h_k$ is a function ($h_k : \mathbb{R}^{2SN_\theta} \rightarrow \mathbb{R}^L$) defining the relationship between the boundary vector and measured vector and the measured voltages for the $k$the current pattern. The measurement error $v_k \in \mathbb{R}^L$ is assumed to be white Gaussian noise with the covariance $R_k$. Linearizing Eq. (7) about the predicted (time-updated) state $\gamma_{k|k-1}$, described later (section 3.1), we obtain

$$\bar{u}_k = h_k(\gamma_{k|k-1}) + J_k(\gamma_{k|k-1}) \cdot (\gamma_k - \gamma_{k|k-1}) + H.O.Ts + v_k \tag{8}$$

where $H.O.Ts$ represents the higher-order terms which are assumed to be additional white Gaussian noise, and $J_k(\gamma_{k|k-1}) \in \mathbb{R}^{L \times 2SN_\theta}$ is the Jacobian matrix defined by

$$J_k(\gamma_{k|k-1}) \equiv \left.\frac{\partial h_k}{\partial \gamma}\right|_{\gamma = \gamma_{k|k-1}} \tag{9}$$

Let's define a pseudo-measurement as

$$y_k \equiv \bar{u}_k - h_k(\gamma_{k|k-1}) + J_k(\gamma_{k|k-1}) \cdot \gamma_{k|k-1} \tag{10}$$

Then we can obtain the following linearized measurement equation:

$$y_k = J_k(\gamma_{k|k-1}) \cdot \gamma_k + \bar{v}_k \tag{11}$$

where $\bar{v}_k \in \mathbb{R}^L$ is composed of the measurement error and linearization error with known covariance as $\bar{R}_k$.

### 3.1. Extended Kalman Filter Formulation

In Kalman filtering we estimate the state vector $\gamma_k$ based on all the measurements taken up to time $kT$. With the Gaussian assumptions the required estimate is obtained by minimizing the cost functional which is formulated based on the above state and measurement equations. Eq. (5) and Eq. (11), respectively.

$$\aleph(\gamma_k)=\frac{1}{2}[\,||\gamma_k-\gamma_{k|k-1}||_{(C_{k|k-1})^{-1}} +||y_k-J_k(\gamma_{k|k-1})\cdot\gamma_k||_{R_k^{-1}}+\alpha||R(\gamma_k-\gamma^*)||\,] \tag{12}$$

where $||\cdot||_A$ denotes $x^TAx$, $\alpha$ and $R\in\mathbb{R}^{2SN_\theta\times 2SN_\theta}$ are the regularization parameter and regularization matrix, respectively, $\gamma^*$ is an a priori guess for the boundary representation, and $C_{k|k-1}\in\mathbb{R}^{2SN_\theta\times 2SN_\theta}$ is the time-updated error covariance matrix, which is given by

$$C_{k|k-1}=E[(\gamma_k-\gamma_{k|k-1})(\gamma_k-\gamma_{k|k-1})^T] \tag{13}$$

and measurement matrix $H_k\in\mathbb{R}^{(L+2SN_\theta)\times 2SN_\theta}$. The first two norms in Eq. (12) refer to the weighted norms, having as weighting matrices the inverse of the covariances. The third term on the right-hand side of Eq. (12) is the regularization term which is included to mitigate the ill-posedness of the given problem. We used the generalized Tikhonov regularization under a smoothness assumption in constructing the regularization matrix ($R$), with the regularization parameter $\alpha$ chosen empirically. If we define the augmented pseudo-measurement $\bar{y}_k\in\mathbb{R}^{(L+2SN_\theta)}$ and measurement matrix

$$\bar{y}_k\equiv\begin{pmatrix} y_k \\ \sqrt{\alpha}R\gamma^* \end{pmatrix} \tag{14}$$

$$H_k\equiv\begin{pmatrix} J_k(\gamma_{k|k-1}) \\ \sqrt{\alpha}R \end{pmatrix} \tag{15}$$

then the cost functional Eq. (12) can be re-arranged as

$$\aleph(\gamma_k)=\frac{1}{2}[\,||\gamma_k-\gamma_{k|k-1}||_{(C_{k|k-1})^{-1}} +||\bar{y}_k-H_k\cdot\gamma_k||_{\Gamma_k^{-1}}\,] \tag{16}$$

where $\Gamma_k\in\mathbb{R}^{(L+2SN_\theta)\times(L+2SN_\theta)}$ is a block diagonal matrix defined by

$$\Gamma_k\equiv Blockdiag[\bar{R}_k, I_{2SN_\theta}] \tag{17}$$

Minimizing the cost functional Eq. (16) and solving for the updates of the associated covariance matrices, we obtain the recursive extended Kalman filter algorithm, which consists of the following two steps in [10]:
time update (prediction)

$$\gamma_{k+1|k}=F_k\gamma_{k|k} \tag{18}$$

$$C_{k+1|k}=F_kC_{k|k}(F_k)^T+Q_k \tag{19}$$

measurement update (filtering)

$$G_{k+1|k}=C_{k+1|k}(H_{k+1})^T[H_{k+1}C_{k+1|k}(H_{k+1})^T+\Gamma_{k+1}]^{-1} \tag{20}$$

$$\gamma_{k+1|k+1}=\gamma_{k+1|k}+G_{k+1}(\bar{y}_{k+1}-H_{k+1}\gamma_{k+1|k}) \tag{21}$$

$$C_{k+1|k+1}=(I_{2SN_\theta}-G_{k+1}H_{k+1})C_{k+1|k} \tag{22}$$

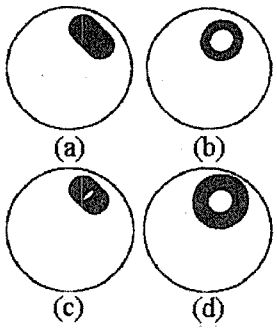


Fig. 1 Simulation Scenarios: (a) Bubble is moving with constant velocity; (b) Bubble is expanding with constant velocity; (c) Bubble is moving with constant acceleration; and (d) Bubble is expanding with constant acceleration. Transient boundaries are superimposed onto each other.

## 4. Numerical Results with Kinematic Model

In order to evaluate the performance of the proposed approach, we have considered four different scenarios for phase boundaries as shown in Fig. 1. The elliptic object undergoes a transient change in a circular domain (30cm in diameter) after each current pattern ($\triangle t = 0.01sec$). The trignometric current patterns were injected into the domain. Reading for 3 image frames were acquired (93 current injections). In all the scenarios, the object and the background resistivities were set to $250 \times 10^6 \Omega cm$ and $250 \Omega cm$ respectively, so that the contrast ratio between the object and the background is $10^6 : 1$. We assumed a very high contrast ratio here since the final goal of this research is to estimate the boundaries of bubbles in a liquid. Here, we adopt the kinematic model (KM) for the state equation Eq. (5), which takes into account the first- and second-order derivatives of $\gamma$ of the shape of coefficients. Originally, the KMs were developed for the target tracking field [11] to estimate the maneuvering target, in which the acceleration and the jerk are considered as white Gaussian noise for the first- and second-order kinematic model, respectively.

For a bubble moving with constant velocity (Simulation 1), the required state vector, state matrix and measurement matrix are as follows:

$$\gamma = [\ \gamma_1^{x_1}\ \dot{\gamma}_1^{x_1}\ \gamma_1^{y_1}\ \dot{\gamma}_1^{y_1}\ \gamma_1^{x_2}\ \gamma_1^{y_2}\ \gamma_1^{x_3}\ \gamma_1^{y_3}\ ]^T \tag{23}$$

$$F_k = \begin{bmatrix} 1 & \triangle t & 0 & 0 & 0 & 0 & 0 \\ 0 & 1 & 0 & 0 & 0 & 0 & 0 \\ 0 & 0 & 1 & \triangle t & 0 & 0 & 0 \\ 0 & 0 & 0 & 1 & 0 & 0 & 0 \\ 0 & 0 & 0 & 0 & 1 & 0 & 0 \\ 0 & 0 & 0 & 0 & 0 & 1 & 0 \\ 0 & 0 & 0 & 0 & 0 & 0 & 1 \end{bmatrix} \tag{24}$$

$$H_k = \begin{bmatrix} J_k^{(1,1)} & 0 & J_k^{(1,2)} & 0 & J_k^{(1,3)} & J_k^{(1,4)} & J_k^{(1,5)} & J_k^{(1,6)} \\ J_k^{(2,1)} & 0 & J_k^{(2,2)} & 0 & J_k^{(2,3)} & J_k^{(2,4)} & J_k^{(2,5)} & J_k^{(2,6)} \\ \vdots & \vdots & \vdots & \vdots & \vdots & \vdots & \vdots & \vdots \\ J_k^{(32,1)} & 0 & J_k^{(32,2)} & 0 & J_k^{(32,3)} & J_k^{(32,4)} & J_k^{(32,5)} & J_k^{(32,6)} \end{bmatrix} \tag{25}$$

For a bubble expanding with constant velocity (Simulation 2), the required state vector, state matrix and measurement matrix are as follows:

$$\gamma = [\ \gamma_1^{x_1}\ \gamma_1^{y_1}\ \gamma_1^{x_2}\ \dot{\gamma}_1^{x_2}\ \gamma_1^{y_2}\ \gamma_1^{x_3}\ \gamma_1^{y_3}\ \dot{\gamma}_1^{y_3}\ ]^T \tag{26}$$

$$F_k = \begin{bmatrix} 1 & 0 & 0 & 0 & 0 & 0 & 0 \\ 0 & 1 & 0 & 0 & 0 & 0 & 0 \\ 0 & 0 & 1 & \triangle t & 0 & 0 & 0 \\ 0 & 0 & 0 & 1 & 0 & 0 & 0 \\ 0 & 0 & 0 & 0 & 1 & 0 & 0 \\ 0 & 0 & 0 & 0 & 0 & 1 & \triangle t \\ 0 & 0 & 0 & 0 & 0 & 0 & 1 \end{bmatrix} \tag{27}$$

$$H_k = \begin{bmatrix} J_k^{(1,1)} & J_k^{(1,2)} & J_k^{(1,3)} & 0 & J_k^{(1,4)} & J_k^{(1,5)} & J_k^{(1,6)} & 0 \\ J_k^{(2,1)} & J_k^{(2,2)} & J_k^{(2,3)} & 0 & J_k^{(2,4)} & J_k^{(2,5)} & J_k^{(2,6)} & 0 \\ \vdots & \vdots & \vdots & \vdots & \vdots & \vdots & \vdots & \vdots \\ J_k^{(32,1)} & J_k^{(32,2)} & J_k^{(32,3)} & 0 & J_k^{(32,4)} & J_k^{(32,5)} & J_k^{(32,6)} & 0 \end{bmatrix} \tag{28}$$

For a bubble moving with constant acceleration (Simulation 3), the required state vec-

tor, state transition matrix and measurement matrix are as follows:

$$\gamma = [\ \gamma_1^{x_1}\ \dot{\gamma}_1^{x_1}\ \ddot{\gamma}_1^{x_1}\ \gamma_1^{y_1}\ \dot{\gamma}_1^{y_1}\ \ddot{\gamma}_1^{y_1}\ \gamma_1^{x_2}\ \gamma_1^{y_2}\ \gamma_1^{x_3}\ \gamma_1^{y_3}\ ]^T \tag{29}$$

$$F_k = \begin{bmatrix} 1 & \triangle t & \frac{1}{2}\triangle t^2 & 0 & 0 & 0 & 0 & 0 & 0 & 0 \\ 0 & 1 & \triangle t & 0 & 0 & 0 & 0 & 0 & 0 & 0 \\ 0 & 0 & 1 & 0 & 0 & 0 & 0 & 0 & 0 & 0 \\ 0 & 0 & 0 & 1 & \triangle t & \frac{1}{2}\triangle t^2 & 0 & 0 & 0 & 0 \\ 0 & 0 & 0 & 0 & 1 & \triangle t & 0 & 0 & 0 & 0 \\ 0 & 0 & 0 & 0 & 0 & 1 & 0 & 0 & 0 & 0 \\ 0 & 0 & 0 & 0 & 0 & 0 & 1 & 0 & 0 & 0 \\ 0 & 0 & 0 & 0 & 0 & 0 & 0 & 1 & 0 & 0 \\ 0 & 0 & 0 & 0 & 0 & 0 & 0 & 0 & 1 & 0 \\ 0 & 0 & 0 & 0 & 0 & 0 & 0 & 0 & 0 & 1 \end{bmatrix} \tag{30}$$

$$H_k = \begin{bmatrix} J_k^{(1,1)} & 0 & 0 & J_k^{(1,2)} & 0 & 0 & J_k^{(1,3)} & J_k^{(1,4)} & J_k^{(1,5)} & J_k^{(1,6)} \\ J_k^{(2,1)} & 0 & 0 & J_k^{(2,2)} & 0 & 0 & J_k^{(2,3)} & J_k^{(2,4)} & J_k^{(2,5)} & J_k^{(2,6)} \\ \vdots & \vdots & \vdots & \vdots & \vdots & \vdots & \vdots & \vdots & \vdots & \vdots \\ J_k^{(32,1)} & 0 & 0 & J_k^{(32,2)} & 0 & 0 & J_k^{(32,3)} & J_k^{(32,4)} & J_k^{(32,5)} & J_k^{(32,6)} \end{bmatrix} \tag{31}$$

For a bubble expanding with constant acceleration (Simulation 4), the required state vector, state transition matrix and measurement matrix are as follows:

$$\gamma = [\ \gamma_1^{x_1}\ \gamma_1^{y_1}\ \gamma_1^{x_2}\ \dot{\gamma}_1^{x_2}\ \ddot{\gamma}_1^{x_2}\ \gamma_1^{y_2}\ \gamma_1^{x_3}\ \gamma_1^{y_3}\ \dot{\gamma}_1^{y_3}\ \ddot{\gamma}_1^{y_3}\ ]^T \tag{32}$$

$$F_k = \begin{bmatrix} 1 & 0 & 0 & 0 & 0 & 0 & 0 & 0 & 0 & 0 \\ 0 & 1 & 0 & 0 & 0 & 0 & 0 & 0 & 0 & 0 \\ 0 & 0 & 1 & \triangle t & \frac{1}{2}\triangle t^2 & 0 & 0 & 0 & 0 & 0 \\ 0 & 0 & 0 & 1 & \triangle t & 0 & 0 & 0 & 0 & 0 \\ 0 & 0 & 0 & 0 & 1 & 0 & 0 & 0 & 0 & 0 \\ 0 & 0 & 0 & 0 & 0 & 1 & 0 & 0 & 0 & 0 \\ 0 & 0 & 0 & 0 & 0 & 0 & 1 & 0 & 0 & 0 \\ 0 & 0 & 0 & 0 & 0 & 0 & 0 & 1 & \triangle t & \frac{1}{2}\triangle t^2 \\ 0 & 0 & 0 & 0 & 0 & 0 & 0 & 0 & 1 & \triangle t \\ 0 & 0 & 0 & 0 & 0 & 0 & 0 & 0 & 0 & 1 \end{bmatrix} \tag{33}$$

$$H_k = \begin{bmatrix} J_k^{(1,1)} & J_k^{(1,2)} & J_k^{(1,3)} & 0 & 0 & J_k^{(1,4)} & J_k^{(1,5)} & J_k^{(1,6)} & 0 & 0 \\ J_k^{(2,1)} & J_k^{(2,2)} & J_k^{(2,3)} & 0 & 0 & J_k^{(2,4)} & J_k^{(2,5)} & J_k^{(2,6)} & 0 & 0 \\ \vdots & \vdots & \vdots & \vdots & \vdots & \vdots & \vdots & \vdots & \vdots & \vdots \\ J_k^{(32,1)} & J_k^{(32,2)} & J_k^{(32,3)} & 0 & 0 & J_k^{(32,4)} & J_k^{(32,5)} & J_k^{(32,6)} & 0 & 0 \end{bmatrix} \tag{34}$$

Table 1. Extended Kalman filter parameters.

| | Simulation 1 | Simulation 2 | Simulation 3 | Simulation 4 |
|---|---|---|---|---|
| $Q_k$ | $I_8$ | $I_8$ | $I_{10}$ | $I_{10}$ |
| $R_k$ | $200I_{32}$ | $200I_{32}$ | $200I_{32}$ | $200I_{32}$ |
| $C_{0\|0}$ | $I_8$ | $I_8$ | $I_{10}$ | $I_{10}$ |

The EKF parameters used in the simulations are shown in Table 1 The regularization parameter $\alpha$ was set to 0.1. Furthermore, in all simulations, zero-mean Gaussian noise was added to the calculated voltages to generate noisy measurements; the noise level was set to be 1% of the corresponding calculated voltages. The reconstruction results for the simulations are shown in Fig. 2 in which the columns represent the true and estimated profile after 15 current injections. In Fig. 3 root mean square error (RMSE) comparison for region boundaries is done between KM and random-walk model for a monte-carlo simulation of 10 runs for each scenario. From the results it should be pointed out that the estimation performance of the EKF with KM is better than random-walk model in most cases. For the case when bubble is moving with constant velocity, there is a significant difference in RMSE values of KM and random-walk model between $40th$ and $80th$ current patterns and for the bubble expanding with constant acceleration, there is a significant difference between $35th$ and $75th$ current patterns.

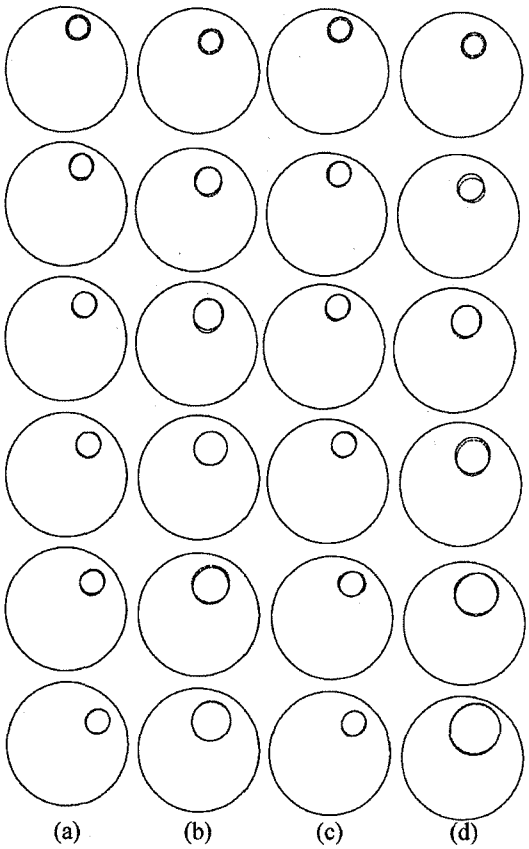


Fig. 2 Reconstruction results with KMs: (a) Bubble is moving with constant velocity; (b) Bubble is expanding with constant velocity; (c) Bubble is moving with constant acceleration; and (d) Bubble is expanding with constant acceleration. Solid line represents the true boundary whereas the dotted line represents the estimated boundary.

## 5. Conclusions

In this paper, we have addressed a special class of the EIT inverse problem, in which position and shape of the objects (bubble in this case) were the unknowns to be identified while resistivities of the objects are known a priori. The boundary of the object was formulated as truncated Fourier series, and time-varying Fourier coefficients were estimated with the aid of extended Kalman filter, following the voltage measurements corresponding to each current pattern. Different kinematic models were considered for modeling different behaviors of air bubble. Comparison was done with conventional random-walk model to evaluate the performance.

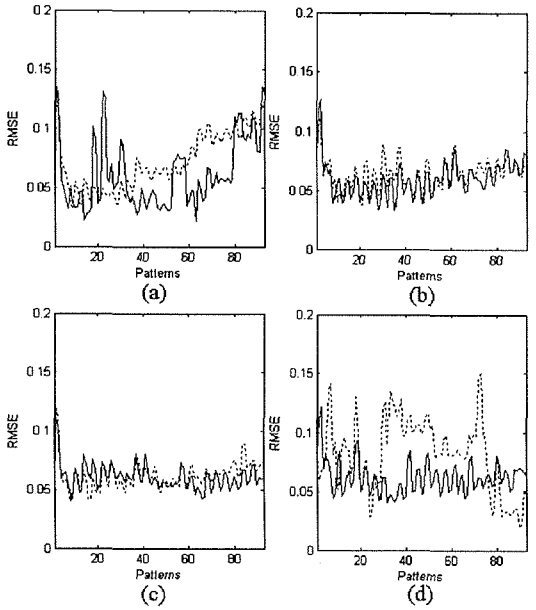


Fig. 3 RMSE comparison with monte-carlo simulations of 10 runs: (a) Bubble is moving with constant velocity; (b) Bubble is expanding with constant velocity; (c) Bubble is moving with constant acceleration; and (d) Bubble is expanding with constant acceleration. Solid line represents the RMSE with KM whereas dotted line represents the RMSE with random-walk model.

## Acknowledgment

This research is supported by the grant from "the 2nd phase BK21 project"

## References


[1] Butler, J.E., Bonnecaze, R.T., 2000, Inverse method for imaging a free surface using electrical tomography, Chemical Engineering Science, Vol.55, pp.1193-1204.

[2] Chan, T.F., Tai, X.C., 2004, Level set and total variation regularization for elliptic inverse problems with discontinuous coefficients, Journal of Computational Physics, Vol.193, No.1, pp.40-66.

[3] Kolehmainen, V., Arridge, S.R., Lionhart, W.R.B., Vauhkonen, M., Kaipio, J.P., 1999, Recovery of region boundaries of piecewise constant coefficients of an elliptic PDE from boundary data, Inverse Problems, Vol.15, pp.1375-1391.

[4] Kim, M.C., Lee, K.J., Kim, S., Kim, K.Y., 2004, Improvement of the electrical impedance tomographic image for the two-phase system with adaptive element grouping technique, Measurement Science and Technology, Vol.15, pp.1391-1401.

[5] Kim, M.C., Kim, K.Y., Kim, S., 2004, Improvement of impedance imaging for two-phase systems with boundary estimation approach in electrical impedance tomography, Canadian Journal of Chemical Engineering, Vol.83, pp.55-63.

[6] Kim, M.C., Kim, K.Y., Kim, S., 2004, Estimation of phase boundaries in two-phase systems by electrical impedance tomography technique. Journal of Industrial and Engineering Chemistry, The Korean Society of Industrial and Engineering Chemistry, Vol.10, pp.710-716.

[7] Tossavainen, O.P., Kolehmainen, V., Vauhkonen, M., 2006, Free-surface and admittivity estimation in electrical impedance tomography, International Journal for Numerical Methods in Engineering, Vol.66, pp.1991-2013.

[8] Han, D.K., Prosperetti, A., 1999, A shape decomposition technique in electrical impedance tomography, Journal of Computational Physics, Vol.155, pp.75-95.

[9] Kolehmainen, V., Voutilainen, A., Kaipio, J.P., 2001, Estimation of non-stationary region boundaries in EIT-state estimation approach, Inverse Problems, Vol.17, pp. 1937-1956.

[10] Gelb, A., 1974, Applied Optimal Estimation. The MIT Press, Massachusetts.

[11] Bar-Shalom, Y. et al., 1993, Estimation in Tracking, Principles, Techniques, and Softwares. Artech House, London.